Dynamics of bulk-to-surface electron transitions on Si(001)-(2×1) studied by time-resolved two-photon photoemission spectroscopy

S. Tanaka, T. Ichibayashi, and K. Tanimura

The Institute of Scientific and Industrial Research, Osaka University, 8-1 Mihogaoka, Ibaraki, Osaka 567-0047, Japan

(Received 27 October 2008; revised manuscript received 23 February 2009; published 20 April 2009)

The carrier dynamics on Si(001)-(2×1) have been studied by means of time- and angle-resolved two-photon photoemission spectroscopies at 291 K. Temporal changes in electron populations at the normally unoccupied surface band (D_{down}) and at the bulk conduction-band minimum (CBM) have been probed simultaneously to characterize the pathways of bulk-to-surface electron transfer. The decay kinetics of the electron population at the bottom of D_{down} and at the CBM, obtained at two different excitation wavelengths, where the bulk absorption coefficient differs significantly, show a strong dependence on wavelength. Analysis shows that the dependence of the population at the CBM is characterized by carrier diffusion away from the surface and by rapid surface recombination, with a surface-recombination velocity of 1.2×10^6 cm/s. The surface-recombination pathway from the CBM to the high-lying state along the $\bar{\Gamma}-\bar{J}'$ dispersive branch of the D_{down} band has been directly probed by an angle-resolved technique. Quantitative comparisons of electron flows into the D_{down} band and the decay kinetics of the population of the bottom of D_{down} reveal an efficient quadratic decay channel of the surface electron-hole recombination.

DOI: 10.1103/PhysRevB.79.155313 PACS number(s): 73.20.At, 79.60.Bm, 79.60.Dp, 79.60.Ht

I. INTRODUCTION

Ultrafast carrier dynamics in semiconductors are of great scientific and technological interest. A comprehensive understanding of ultrafast carrier relaxation is needed to determine the mechanisms of several striking effects caused by ultrashort laser interactions with solids, including nonthermal melting,[1–3] photoinduced phase transition,[4–6] and electronic ablation.[7–9] The continuing miniaturization of semiconductor devices into the nanoscale regime requires a clear understanding of the dynamics near surfaces and interfaces at an increasingly shorter time scale. It is evident that hot-carrier dynamics, including coupling of bulk electrons to surface and interface states, governs the dominant pathways of recombination processes.[10,11] Previous time-resolved spectroscopic studies have established three primary ultrafast processes of carrier relaxation, at least conceptually:[12–14] the momentum-relaxing scattering to dephase excited-carrier states, electronic thermalization to establish quasiequilibrated electronic states, and energy relaxation to thermalize hot carriers with the lattice. In combination with carrier diffusion[15] and drift transport, induced by transient space charging,[16] these processes govern carrier scattering into surface states. Despite accumulating knowledge, no clear picture of the ultrafast dynamical coupling of bulk electrons to intrinsic Si surface states has emerged.

Time-resolved two-photon photoemission spectroscopy (TR-2PPE) is one of the most powerful methods for studying ultrafast surface carrier dynamics.[17] Adding angle-resolved measurements to this method provides time-resolved photoemission spectroscopy for determination of energy- and momentum-resolved dynamics of surface states. By carefully tuning the photon energy ($h\nu_{prob}$) of probe pulses below the work function Φ_{vac}, the strong background coming from one-photon photoemission may be suppressed, thus reducing possible space-charge effects on low-energy electron detection and enhancing spectral resolution of low-energy peaks. Also, this method allows us to access both occupied and unoccupied surface states in a single experiment to eliminate reference-level problems.[18] The use of low-photon energy probe light is not typical for studying bulk-electronic states in photoemission spectroscopy and has created some difficulties in measuring their dynamics.[19] However, a recent two-photon photoemission spectroscopy (2PPE) study has shown that the photoemission from the bulk conduction-band minimum (CBM) in Si is readily detectable by the surface photoelectric effect via the inverse low energy electron diffraction (LEED) state even for $h\nu_{prob}$'s less than Φ_{vac}.[20] Thus, it is now possible to study carrier dynamics on Si surfaces while detecting surface- and bulk-electronic states simultaneously. Here we detail a TR-2PPE study of the important Si(001)-(2×1) surface, the basis of most of present-day semiconductor devices, which elucidates the dynamics of bulk-to-surface electron transitions.

The surface structure of Si(001)-(2×1) is characterized by asymmetric Si surface dimers. Depending on the competition between the thermal excitation of the dimer rocking mode and long-range order formation, the surface takes either a $c(4\times2)$ structure below 200 K or a (2×1) structure above this temperature, separated by a reversible second-order phase transition.[21] The dangling bonds of asymmetric Si dimers form two distinct surface electronic bands: a filled dangling-bond band (D_{up}) and an empty band (D_{down}).[22] Reflecting the dimer-row configuration of this surface, these dangling-bond bands show a quasi-one-dimensional feature; exhibiting a large dispersion along the chain direction. In contrast there is almost no dispersion perpendicular to the chain direction,[23–25] as shown schematically in Fig. 1. The energetics of these intrinsic surface states have been studied extensively by 2PPE spectroscopy and through quasiparticle many-body calculations.[24,25] The electronic properties of Si(001)-(2×1) above 200 K are essentially the same as those of Si(001)-$c(4\times2)$.[25] Weinelt *et al.*[24] studied ultrafast surface-carrier dynamics on Si(001)-$c(4\times2)$ at 90 K using

 ©2009 The American Physical Society

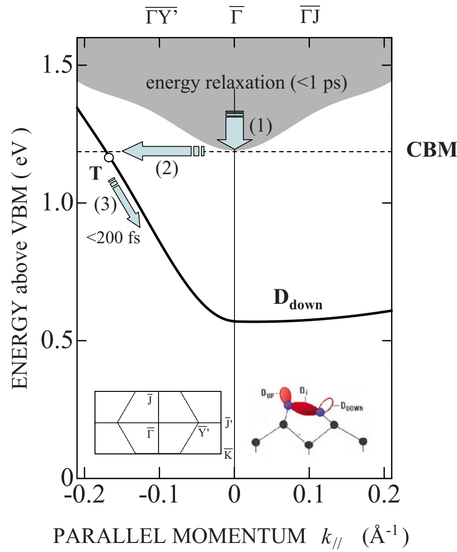

FIG. 1. (Color online) Schematic drawing of the electronic structure of Si(001)-(2×1). Shaded area marks the projected bulk conduction band and the solid curve is the dispersion of the normally unoccupied dangling-bond band (D_{down}) (Ref. 24). Point T represents a high-lying level on the dispersive branch of the D_{down} band. Arrows show possible processes in the bulk-to-surface electron transition. Arrows (1), (2), and (3) represent the energy relaxation process of hot electrons near the CBM, the bulk-to-surface state transition, and intraband relaxation of the D_{down} band. Inset: A schematic model of an asymmetric Si dimer on the surface. The D_{down} band is composed of the unoccupied dangling bond labeled D_{down}. Surface Brillouin zone for the (2×1) structure, solid line, and for the $c(4\times2)$ structure, dotted line, are shown as well.

angle- and time-resolved 2PPE and characterized important features of ultrafast surface-band relaxation and the formation of a new state assigned to be the surface exciton. However, an excitation-density dependent growth rate and excitation-wavelength dependent decay kinetics of normally unoccupied D_{down} band have been reported for Si(001)-(2×1) at room temperature,[26,27] both of which cannot be described in terms of relaxations within surface-specific electronic states. Instead, these observations suggest the important role of bulk-to-surface electron transfer in surface-band dynamics. However, a detailed understanding of these dynamics remains unclear for this surface.

In this paper, we report comprehensive carrier dynamics of Si(001)-(2×1) studied by time- and angle-resolved 2PPE spectroscopies where we simultaneously probe both the bulk electrons accumulated near the CBM and the transiently populated electrons in the normally unoccupied surface state of D_{down}. Results obtained at two different excitation wavelengths, where the bulk absorption coefficient differs significantly, reveal that the decay of electron population at the CBM is characterized by carrier diffusion away from the surface and by surface recombination, showing a strong excitation-wavelength dependence. The surface-recombination pathway from the CBM to the high-lying state along the $\bar{\Gamma}-\bar{J}'$ dispersive branch of the D_{down} band is directly probed using the angle-resolved technique. Comparisons of the experimentally detected electron flows into the high-lying D_{down} state and the decay kinetics of the population at the bottom of D_{down} at the $\bar{\Gamma}$ point in the surface Brillouin zone clearly reveal an efficient quadratic decay channel of the surface electron-hole recombination.

II. EXPERIMENT

The experiments were carried out in an ultrahigh-vacuum (UHV) system consisting of three chambers: one equipped with an electron analyzer for 2PPE, the second with an STM for surface characterization, and the third for sample preparation. Base pressures of the three chambers were 5×10^{-11} Torr, 3×10^{-11} Torr, and 4×10^{-11} Torr, respectively. Boron-doped p-type Si(001) wafers (10 Ω cm) were clamped with Ta sheets to the sample holder and were transferred from one to the other in UHV. The samples were cleaned by resistive heating at about 1100 °C for about 10 s with a pressure below 8×10^{-11} Torr and then slowly cooled down to room temperature with a rate less than - 10 °C/s. STM analysis of the surface structures prior to photoemission measurements confirmed a well-ordered (2×1) double-domain structure with surface-defect concentrations of less than 1%. The ratio of the two domains was dependent on the sample history and cleaning conditions.

In the 2PPE experiments, the pump pulse was the fundamental (730 nm, referred to as ω hereafter), or the second harmonic (365 nm, 2ω hereafter), generated by a mode-locked Ti:sapphire laser operating at a 76 MHz repetition rate. The probe pulse was the third harmonic (243.3 nm, 3ω) of the fundamental, generated using beta-barium borate crystals. Temporal widths of ω and 2ω pump pulses were 140 fs and that of the 3ω probe pulses were 160 fs. The cross-correlation trace of pump and probe pulses showed typically 220 fs temporal width (full width at half maxima) at the sample position in the UHV chamber. Probe pulses were strictly p polarized, while the pump pulses were either s or p polarized. These pulses with a preset time delay (Δt) were aligned coaxially and were focused on surfaces with a quartz lens. The incident angle of the laser light was 45° with respect to the axis of the photoelectron analyzer of hemispherical type. The angle-resolved measurement was accomplished by rotating the sample along the (011) direction such that the angle between the surface normal and the incidence beam was decreased. Emitted electrons were analyzed by a hemispherical analyzer with an energy resolution of 70 meV and an angular resolution of ±2°.

III. RESULTS

Figure 2 shows the time-resolved 2PPE spectra of Si(001)-(2×1) surfaces at 291 K, measured for (a) s-polarized ω-pump pulses and for [(b) and (c)] s-polarized 2ω-pump pulses. The photon energy $h\nu_{\mathrm{prob}}$ of the p-polarized 3ω-probe pulses was the same for both cases. The energy scale of photoemission spectra is referred to the valence-band maximum (VBM), based on the fact that the flat-band condition is maintained at any Δt's for this p-type surface,[25] and on well-established ionization energy,[18] band-gap energy,[18] and the Fermi levels of the present specimens. In

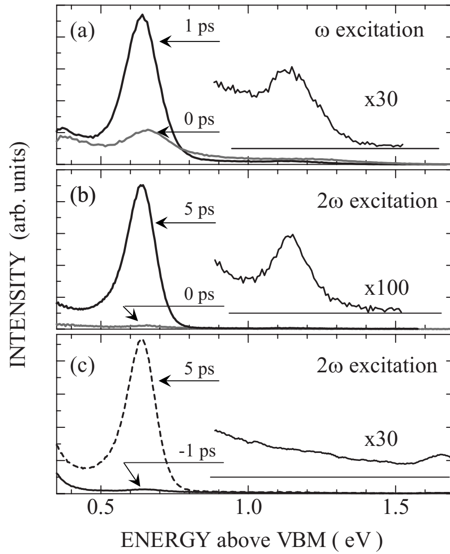

FIG. 2. (a) Time-resolved 2PPE spectra for the s-polarized ω excitation and [(b) and (c)] for the s-polarized 2ω excitation. The energy scale of photoemission spectra is referred to the VBM. In (a) and (b), the spectra, measured for electrons emitted along the surface normal, at the Δt's indicated, are displayed after subtracting the spectrum at $\Delta t = -1$ ps for ω- or 2ω-pump pulse. In (c), the spectra measured at $\Delta t = -1$ ps and at 5 ps are shown for 2ω excitation. Inset shows the spectrum at $\Delta t = 1$ ps in an expanded scale ($\times 30$) in (a), that at $\Delta t = 5$ ps($\times 100$) in (b) and that at -1 ps($\times 30$) in (c).

Fig. 2(c), we show the spectra at $\Delta t = -1$ and 5 ps for the case of 2ω excitation. The spectrum at $\Delta t = -1$ ps represents the residual effects due to preceding pump pulses (13.16 ns interval) and pump-pulse-induced multiphoton photoemission components. In the spectrum, the low-energy component below $E = 0.4$ eV has been ascribed to the photoemission from surface defects by 3ω-probe pulses and the similar low-energy peak is detected in the spectrum at $\Delta t = -1$ ps for the ω-excitation case (not shown). Although the photon energy of the 2ω pulse is significantly lower than the work function of the Si(001) surface,[10] it can generate coherent two-photon photoemission, with a peak feature at 1.66 eV, in the whole energy region as seen in the inset shown at an expanded scale.[27] The intensity of the coherent peaks is not dependent on Δt's and is significantly weak compared to pump-pulse induced peaks. Therefore, the spectrum at $\Delta t = -1$ ps can be regarded as the "background" in the time-resolved measurements. The subtraction of the spectrum at $\Delta t = -1$ ps from the measured spectra for ω or 2ω-pump pulses eliminates residual effects due to preceding pump pulses and pump-pulse-induced photoemission components to emphasize the pump-pulse induced effects in the photoemission spectra. The spectra in Figs. 1(a) and 1(b) at Δt's indicated are thus displayed after subtracting the spectrum at $\Delta t = -1$ ps for ω- or 2ω-excitation case.

In Figs. 2(a) and 2(b), the peak 0.64 eV above the VBM has been assigned to the D_{down} state at $\bar{\Gamma}$, $D_{down}(\bar{\Gamma})$ hereafter, the bottom of this normally unoccupied surface band. The $D_{down}(\bar{\Gamma})$ is transiently populated, following the pump pulse, reaching a maximum intensity at a few ps after excitation. The low-intensity peak at 1.14 eV has been assigned to photoemission from the CBM due to the surface photoelectric effect via the inverse LEED state.[20] Therefore, temporal changes in electron populations both at the D_{down} and at the bulk CBM may be probed simultaneously. The 2ω excitation is too high in photon energy to induce direct optical transitions between surface dangling-bond bands,[23] while it efficiently induces bulk valence transitions because of the larger absorption coefficient.[28] The population of the D_{down} state under 2ω-excitation therefore suggests that efficient bulk-to-surface electron transfer is involved in populating $D_{down}(\bar{\Gamma})$.

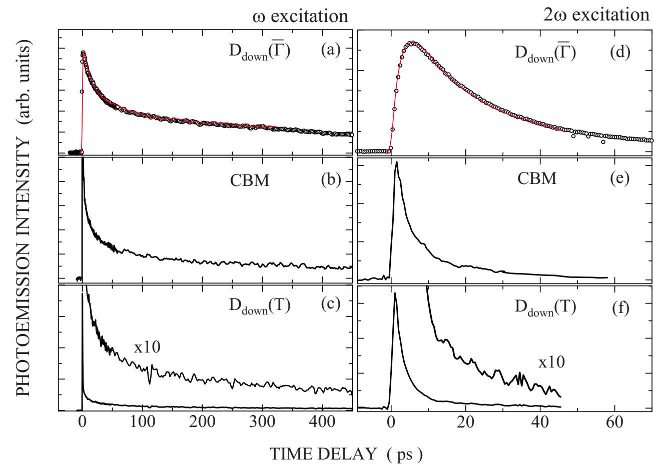

FIG. 3. (Color online) Temporal changes in the photoemission intensities under p-polarized ω excitation (a) from the bottom of the D_{down}, (b) from the CBM, and (c) from the high-lying level of the dispersive branch of the D_{down}. The changes under s-polarized 2ω excitation for the corresponding peaks for ω excitation shown in (a), (b), and (c) are displayed in (d), (e), and (f). Red curves pertaining data points in (a) and (d) are the calculated decay curves of the photoemission from the D_{down} at $\bar{\Gamma}$ (see text).

Although the D_{down} state is similarly populated by both ω and 2ω excitations, significantly different decay kinetics are exhibited. In Fig. 3, we compare temporal changes in the photoemission intensities measured at the peak of $D_{down}(\bar{\Gamma})$, (a) and (d), and at the CBM, (b) and (e), for ω and 2ω excitations. With ω excitation, the intensity of the $D_{down}(\bar{\Gamma})$ peak lasts for over 400 ps, while the intensity is reduced to undetectable levels at approximately 100 ps for 2ω excitation. The different decay kinetics of the same state, shown in Fig. 3, clearly indicate that decay kinetics are not simply governed by the decay channels at $D_{down}(\bar{\Gamma})$, but that the details of electron injection into the state must be taken into account. It is pointed out here that the electron population at the CBM decays in the similar temporal regions as $D_{down}(\bar{\Gamma})$; the intensity of CBM peak lasts for over 400 ps for the ω excitation, while the intensity is reduced to undetectable levels within 60 ps for 2ω excitation.

The electron injection into normally unoccupied surface states takes place by two different pathways: the direct surface-state transitions and indirect bulk-to-surface transitions. Although the former channel of the D_{down} population has been fully analyzed in Ref. 24, the latter pathways of bulk-to-surface transfer remain uncharacterized. Since the energy difference (0.45 eV) between the CBM and $D_{down}(\bar{\Gamma})$

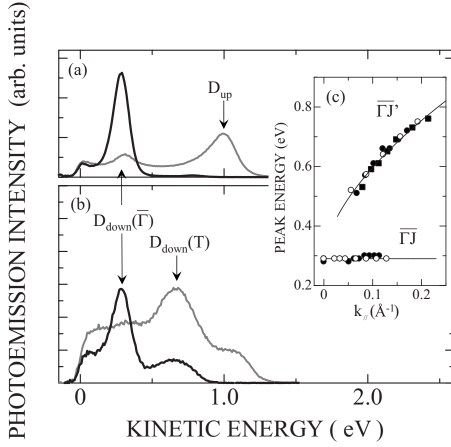

FIG. 4. (a) The time-resolved 2PPE spectra under ω excitation measured in normal emission ($\theta=0°$) at $\Delta t=0$ ps, gray, and $\Delta t=1$ ps, black. (b) The time-resolved 2PPE spectra under ω excitation measured with the off-angle $\theta=20°$ at $\Delta t=0$ ps, gray, and $\Delta t=1$ ps, black. (c) The peak energies of the photoemission peaks from a high-lying level of the dispersive branch D_{down} (T) and the bottom of the D_{down} band as a function of parallel momentum $k_{\|}$, detected for p-polarized ω excitation (○), s-polarized ω excitation (●), and s-polarized 2ω excitation (■).

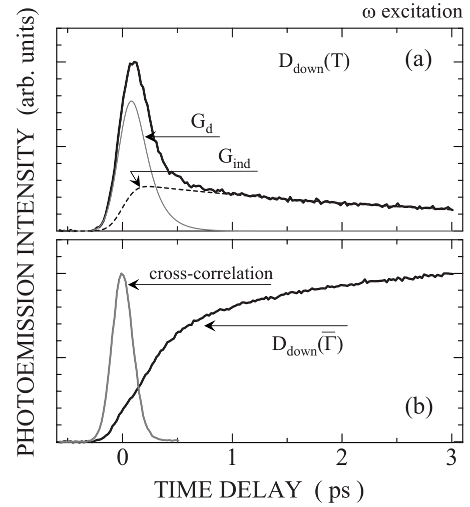

FIG. 5. (a) Temporal changes in photoemission intensity from the high-lying level at the dispersive branch of D_{down} measured at the off-angle of 20°. The gray and broken gray curves are the fit of the rate-equation model (see text). (b) Temporal changes in photoemission intensity from the bottom of D_{down} measured in normal emission. The gray curve shows the cross-correlation trace between pump and probe pulses determined by the temporal evolution of the coherent two-photon photoemission of the 1.0 eV peak in Fig. 4(a).

is significantly larger than available phonon energies, the bulk-to-surface transition which requires energy- and parallel-momentum conservations may take place into a high-lying level of the dispersive branch of the D_{down} band along $\bar{\Gamma}-\bar{J}'$ in the surface Brillouin zone, as schematically shown in Fig. 1. In order to directly trace the transfer process from the CBM to D_{down} we carried out angle-resolved 2PPE measurements to probe temporal electron populations at high-lying states of D_{down}. Because of the double-domain structure of this surface, photoemissions from a high-lying level of the dispersive branch of the D_{down} band and from the D_{down} band at $\bar{\Gamma}$ can be detected simultaneously.[24]

Figure 4(a) shows the 2PPE spectra for the surface-normal emission using p-polarized ω-excitation pulses and 3ω-probe pulses. The energy is scaled with respect to the low-energy cutoff to give the electron kinetic energy E_K. The peak at $E_K=1.0$ eV is two-photon photoemission associated with the image-potential resonance state on this surface.[29] The peak is generated only for p-polarized pump and p-polarized probe pulses and can be used as a measure of the overlap between pump and probe pulses because of the very short lifetime. In Fig. 4(b) we show the photoemission spectra measured at an off-angle θ of 20° for p-polarized ω excitation. An additional peak at $E_K=0.7$ eV, indicated by an arrow, is clearly detected, together with the peak from $D_{\mathrm{down}}(\bar{\Gamma})$ at $E_K=0.3$ eV. With changing θ, the energy of the additional peak moves to the high-energy side, as shown in Fig. 4(c). Here, the wave vector $k_{\|}$ is derived from the formula $k_{\|}=2\pi\sqrt{2mE_K/h^2}\sin\theta$, where h is Planck's constant and m is the electron rest mass. We show the results of dispersions obtained for s-polarized ω-pump pulses (solid circles) at $\Delta t=1$ ps, for p-polarized ω-pump pulses (solid squares) at $\Delta t=1$ ps, and for s-polarized 2ω-pump pulses (open circles) at $\Delta t=1$ ps. The dispersion relation does not depend on the characteristic of the pump pulses and is essentially the same as the relation previously observed.[25] Therefore, we are detecting the temporal population of a high-lying state of D_{down}. The angle θ of 20° corresponds to $k_{\|}=0.15$ Å^{-1} and the state probed at $\theta=20°$ is referred to as state T hereafter (see Fig. 1).

In Fig. 4(b), it is evident that there exists persistent photoemission from state T; a clearly resolved peak is evident at $\Delta t=1$ ps, where pump- and probe-pulse overlaps are entirely negligible. The weak but clearly detectable peak is observed even at $\Delta t=100$ ps (not shown). In order to demonstrate this persistent component more clearly, we show in Fig. 5(a) the temporal evolution of the photoemission intensity from state T. In Fig. 5(b), we also show the cross correlation between pump and probe pulses, determined by the temporal evolution of the 1.0 eV peak in Fig. 4(a).[29] The overlap is approximated by a Gaussian with a width of 220 fs. The emission from state T shows a sharp peak at approximately $\Delta t=0$ with a finite delay and it is associated with a long-lasting persistent component of significant intensity. The peak at approximately $\Delta t=0$ could be attributed to the population due to direct surface-state transitions and/or possible ultrafast hot-electron effects. However, the persistent component extending beyond a few ps cannot be due to the surface transitions since the lifetime of the high-lying state of D_{down} is much less than 1 ps;[24] an analysis suggests the lifetime characterizing the fast decay is around 130 fs as discussed further below. Therefore, the persistent decay component results from an electron flow into the state T from some higher energy states with long lifetimes. In fact, the intensity of the $D_{\mathrm{down}}(\bar{\Gamma})$ shown in Fig. 5(b) continues to increase over a few ps, a much longer duration than the width of the pump pulses and the lifetime of the high-lying levels of D_{down}.

The similar persistent photoemission was detected also for the case of 2ω excitation; the peak energy is plotted in Fig. 4(c) as a function of θ. The temporal changes in the population at state T at longer temporal domains are shown in Figs. 3(c) and 3(f) for ω and 2ω excitations. For ω excitation, the population lasts over 500 ps, while in the case of 2ω excitation it decays within 100 ps, similar to the population at the CBM.

IV. DISCUSSION

A. Excitation-wavelength dependent decay of the electron population at the CBM

As described in Sec. III, temporal evolution of the electron populations at the CBM and surface D_{down} states exhibits a sensitive dependence on the excitation wavelength. We will first discuss the dependence of the CBM-electron population to construct a sound basis on which we can analyze the dependence of the electron populations for the surface states.

The important role of carrier diffusion on photoemission processes in short temporal domains has been discussed previously.[15] In particular, the photoemission from the bulk CBM, under the present experimental conditions, probes only the near-surface region to a depth of about 10 Å.[20] Thus, the diffusion of photogenerated carriers toward the bulk is a crucial factor governing the temporal evolution of the peak intensity. The absorption coefficients α for ω- and 2ω-excitation cases are significantly different: α at 365 nm is 9.32×10^5 cm^{-1}, which is 3 orders of magnitude larger than α at 730 nm (1.8×10^3 cm^{-1}).[28] The steeper concentration gradient generated by 2ω excitation leads to a rapid diffusion away from the surface, leading to the loss of CBM electrons near the surface. A simple estimate of the time τ_D for the average carrier to diffuse a distance equal to the absorption depth[15] for 2ω excitation is 44 fs, while that for ω excitation is as long as 20 ns. Therefore, the electron population at the CBM near surface is reduced not only by surface recombination or electron transfer to surface states, but also by the diffusion into the bulk for 2ω excitation. With ω excitation in this temporal domain, diffusion into the bulk can be neglected and the density gradient produces net transport of electrons toward the surfaces leading to the persistent decay of the CBM photoemission peak. Therefore, the qualitative features shown in Fig. 3 are consistent with what would be expected from electron-diffusion processes.

We have performed numerical calculations based on the diffusion-equation model to further substantiate this conclusion. We use the usual model, in which one assumes a constant electron temperature well equilibrated with lattice temperature, a constant surface-recombination velocity, and an initial carrier distribution as predicted by the absorption coefficient. The limitations and consequences of these approximations are discussed later. In the simulation of the present case, we can neglect the recombination of the carriers within the bulk band since the radiative and Auger recombination processes in Si under the present range of excitation density ($<1\times10^{17}$/cm^3) are much slower.[30] Also, we can ignore the drift current, since the flat-band condition is maintained for p-type specimens of Si(001)-(2×1) under excitation.[25]

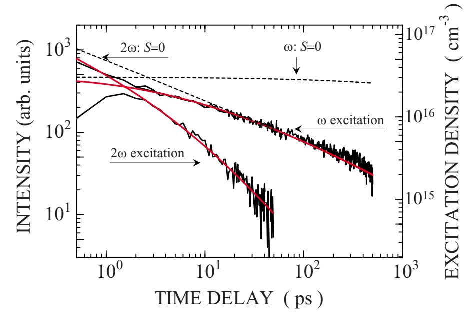

FIG. 6. (Color online) Logarithmic plot of temporal changes in photoemission intensity from the CBM under ω excitation at a fluence of 18.8 μJ/cm^2 and 2ω excitation at a fluence of 0.83 μJ/cm^2. The calculated results, based on the diffusion-equation model, for $S=0$ (broken curves) and for $S=1.2\times10^6$ cm/s (red curves) are compared to the experimental results.

Then, the temporal and spatial changes of the CBM electrons can be described by a one-dimensional diffusion equation

$$\frac{\partial n(z,t)}{\partial t} = \frac{\partial}{\partial z}\left[D\frac{\partial n(z,t)}{\partial z}\right] + G(t)\exp(-\alpha z), \qquad (1)$$

where $n(z,t)$ denotes the density of the CBM electrons in the bulk at a depth z and a time t and D denotes the ambipolar diffusion coefficient. The term of $G(t)\exp(-\alpha z)$ represents the excited electron generation rate by the laser pulse. The above equation is coupled through the boundary condition

$$D\frac{\partial n(z,t)}{\partial z}\bigg|_{z=0} = J_n = Sn(0,t), \qquad (2)$$

where S is the surface-recombination velocity. Although it has been shown that the magnitude of D depends on the carrier density,[13] we used a constant D for the low-density value for simplicity. The diffusion equation was then solved numerically, with a single adjustable parameter S, since the magnitude of D (=18 cm^2 s^{-1}) and the absorption coefficients at the two excitation photon energies were known.[28,30]

The CBM electron density at the surface ($z=0$) simulated by the diffusion-equation model is shown in Fig. 6 and compared to the experimental results of photoemission intensity from the CBM. Since Eq. (1) does not include any density-dependent annihilation terms, the characteristics of temporal change are not dependent on the density. Therefore, the comparison to the experimentally determined decay characteristics of photoemission intensity is straightforward; it needs only a constant normalization factor. The broken curves in Fig. 6 are the simulated results for $S=0$; they simply represent the difference in diffusion effects for the two excitation cases. As discussed above, the electron concentration at the CBM is reduced significantly for the case of 2ω excitation, while it is essentially constant for over 100 ps for the ω excitation. The experimentally detected CBM electron density decays faster than the simulated results for $S=0$, indicating important roles of surface recombination. The results for $S=1.2\times10^6$ cm/s are shown in Fig. 6 by solid curves, together with the experimental results (thick curves) for ω and

2ω excitations. It is evident that the diffusion-equation model with a constant S describes well the measured photoemission decay kinetics of the CBM electrons for temporal range of $\Delta t > 3$ ps.

The diffusion-equation model used in the simulation includes, in principle, some limitations in view of our current understanding of hot carrier dynamics in semiconductors. The hot electrons excited in the X valley via indirect optical transitions undergo energy relaxation to cool the effective temperature of a quasiequilibrated electronic system formed near the CBM within 1 ps of excitation.[31] During the relaxation, electron temperatures are not equilibrated with lattice temperature so that the diffusivity, which is characterized by the mean-free path and an average velocity of electron, and transition rates into the surface states may change over time.[32] In the case of 2ω excitation, we also need to include effects caused by the L-to-X intervalley scattering process, since the photogenerated electrons are injected into the L valley at this excitation energy. At a certain time delay, these dynamical processes may eventually form a given spatial distribution of thermalized electrons that may not be the same as the distribution predicted solely based on the absorption coefficient at the excitation wavelength. Therefore, the diffusion-equation model, in which we assumed a constant electron temperature equilibrated with the lattice and a constant surface-recombination velocity, is not valid for short temporal regime where hot-electron relaxation processes are still underway.

Unfortunately, we cannot describe precisely the effects of hot-electron relaxation on the transport properties at this moment because several important quantities are unavailable. Therefore, we neglected these contributions to the short-time dynamical carrier relaxation in the simulation described above. However, we examined the reliability of the diffusion-equation model by introducing phenomenological and appropriate functions describing time-dependent D, which includes changes in electron temperature, within the first 1 ps,[31] and those related to density-dependent changes.[13] These calculations showed definitely changes in the fast temporal domains within a few ps after excitation, but results in the longer time-delay region (typically 5 ps after excitation) are essentially unchanged. Therefore, we can safely conclude that the decay characteristics of the electron population at the CBM for both ω and 2ω excitations at $\Delta t > 5$ ps are well described by the simple diffusion-equation model associated with a constant surface-recombination velocity.

The successful description of the wavelength-dependent decay kinetics of the CBM electrons described above allows us to draw conclusions about some important characteristics of carrier dynamics on this surface. First, the consistent description of the different decay kinetics in terms of carrier diffusion may substantiate the view that the CBM photoemission peak reflects the properties of bulk-electronic states even though only thin surface layers (~ 10 A) can be probed by the inverse LEED final state. Second, surface recombination on clean Si(001)-(2×1) is characterized by a very high velocity. The surface-recombination velocity of photogenerated carriers for Si surfaces has been evaluated by pump-probe reflectivity measurements.[14] Reported values vary from 10^4 to 10^6 cm/s, depending on sample preparation. Our value using surfaces, with an intrinsic (2×1) structure, corresponds to the highest velocity of those previously reported. This means that electron transitions from the bulk conduction band into surface states, including intrinsic surface specific states and surface-defect states, are very efficient. Third, the diffusion-equation model, using a constant surface-recombination velocity, fails to describe the density changes for the region $\Delta t < 5$ ps. The deviation may be due to the important role of hot-carrier relaxation in bulk-electronic states and/or near surfaces. These issues are important problems for future study.

B. Dynamics of bulk-to-surface electron transfer: microscopic pathways of surface recombination

The decay of CBM electrons at the surface is characterized by a surface-recombination velocity as large as 1.2×10^{-6} cm/s. The microscopic pathway of the recombination is the electron transfer to the surface states including intrinsic surface unoccupied states and surface-defect states. Although the dynamics of electron trapping by surface defects could not be probed directly in this study, we probed electron transitions into the intrinsic surface states of D_{down} by detecting the electron population at the state T, which is a high-lying level on the dispersive branch along the $\bar{\Gamma}-\bar{J}'$ direction of the D_{down} band. The state T, characterized by the off-angle of 20°, corresponds to the level 0.40 eV above $D_{\mathrm{down}}(\bar{\Gamma})$ as shown in Fig. 4(c) and is energetically close to the CBM. Therefore, the population at this state can directly reveal electron flows into the D_{down} band; electrons transferred to this point are relaxed at high rates along the dispersive branch into $D_{\mathrm{down}}(\bar{\Gamma})$.

The temporal profile of the electron population at state T shows a rapid change around $\Delta t = 0$, followed by a persistent decay at $\Delta t > 0.5$ ps. These rapid dynamics may be attributed to direct surface-state optical transitions following fast intraband relaxation, similar to the case at low temperatures,[24] and/or possible ultrafast transitions from hot electrons near the CBM. The persistent component, however, represents indirect electron flows into the D_{down} from states (hereafter referred to as the initial state) located more than 0.4 eV above $D_{\mathrm{down}}(\bar{\Gamma})$.

We initially analyzed the temporal evolution in Fig. 5 in terms of a simple rate-equation model, by which the two different processes can be separated. Two source terms were introduced into the state T: one, $G_d(t)$, is the direct flow component due to the direct optical transition and the other, $D_{\mathrm{ind}}(t)$, is the indirect flow component due to transitions from the initial state with an extended decay time. Since intraband relaxation of state T is well characterized by a single lifetime τ,[24] the electron density n_T of state T can be modeled by

$$\frac{dn_T}{dt} = G_d(t) + G_{\mathrm{ind}}(t) - \frac{1}{\tau} n_T. \quad (3)$$

In this analysis we assume for simplicity that $G_d(t)$ is given by a pump-pulse shape and $G_{\mathrm{ind}}(t)$ is proportional to the population of a state formed directly by a pump pulse with

an apparent decay time (3.7 ps in the temporal domain in Fig. 5). Although the magnitude of τ at 90 K was determined to be 200 fs,[24] we set it an adjustable parameter to fit experimental results. It is expected to be shorter than the low-temperature value because intraband relaxation is a phonon-stimulated process. The gray curve and the broken curves show the best-fit results of the analysis, with τ=130 fs. From the analysis of results obtained for different excitation intensities, we also found that the lifetime of 130 fs was not dependent on the excitation intensity in the range from 1.8 to 45 $\mu J/cm^2$ of ω excitation. Therefore, the relaxation is entirely governed by electron-phonon scattering. Experimental results for other off-angles were analyzed in a similar fashion. As in the case of Ref. 24, τ increases with decreasing θ, consistent with the rate of intraband relaxation along the dispersive branch of D_{down}.[24]

The new finding in this study is the persistent photoemission component from the highly-lying level of the D_{down} band, which clearly shows indirect electron flow into the surface state. This component is incorporated into the function $G_{\mathrm{ind}}(t)$ in Eq. (2). Since the decay time constant of $G_{\mathrm{ind}}(t)$ is much longer than τ at state T, the relationship between $G_{\mathrm{ind}}(t)$ and n_T is given by

$$n_T = \tau G_{\mathrm{ind}}(t), \tag{4}$$

for a temporal domains longer than a few ps, where the direct flow component $G_d(t)$ can be ignored. Therefore, the decay of the photoemission intensity at state T tracks the temporal evolution of the initial state responsible for the persistent electron flow into D_{down} precisely. Calculation of the ratio between the intensities of photoemission from the point T and the CBM, for $\Delta t > 5$ ps, results in a constant value for both ω and 2ω excitation cases. This gives direct evidence for the initial state to be the CBM, revealing a pathway of bulk-to-surface electron transfer in surface recombination.

As clearly shown in Fig. 3, the excitation-wavelength dependent decay kinetics of the $D_{\mathrm{down}}(\bar{\Gamma})$ shows that the kinetics are governed not only by the decay channels at the bottom of the surface band, but also electron flows into the D_{down} state. The advantage of measuring the temporal population at the state T is that it directly yields the electron flow $G(t)[=G_d(t)+G_{\mathrm{ind}}(t)]$ into the D_{down} band. Hence, we can analyze temporal changes in the electron population n_Γ of the $D_{\mathrm{down}}(\bar{\Gamma})$ using the following rate equation:

$$\frac{dn_\Gamma}{dt} = G(t) - \frac{1}{\tau_\Gamma} n_\Gamma - \gamma (n_\Gamma)^2, \tag{5}$$

where $G(t)$ is proportional to the experimentally measured temporal evolution of the photoemission from state T. As decay channels at the $D_{\mathrm{down}}(\bar{\Gamma})$ we introduce linear and quadratic terms, as in the case of other Si surfaces.[16] Several sets of data of temporal changes in the photoemission intensities from the state T and the $D_{\mathrm{down}}(\bar{\Gamma})$, obtained at different excitation wavelengths and intensities, were analyzed in terms of Eq. (5). We were able to fit decay rates that consistently described the results obtained for different excitation characteristics. The solid curves pertaining to data points in Figs. 3(a) and 3(d) are examples of this analysis. The linear term optimized in the analysis is a τ_Γ of 10 ± 1 ps, which may represent the rate of electron trapping by several surface defects. This linear term is of rather long duration and can give a slow growth of the $D_{\mathrm{down}}(\bar{\Gamma})$ population under low-intensity excitation, as observed in Ref. 6. Although it is not possible to determine the absolute magnitude of γ experimentally because of the lack of full occupation of the surface state, the effective decay rate (γn_Γ) becomes 10^{12} s^{-1} for the highest excitation intensity that leads to the bulk excitation density of 10^{17} cm^{-3}.

It has been shown that the flat-band condition is maintained, irrespective of pump-pulse intensities and delay times between pump and probe pulses for p-type Si(001) surface,[24,25] indicating the charge neutrality is hold for this surface. In fact, we confirmed that the low-energy cutoff of the 2PPE spectra, which was sensitive to the band bending, was constant for any Δt's in the present study. The charge neutrality requires that the same densities of electrons and holes are populated in the surface region.[22] Because of the ambipolar diffusion of photogenerated electrons and holes in the bulk region, which implies the same surface-recombination velocities for electrons and holes, the charges in the bulk region beneath the surface may be kept neutral. Therefore, we may assume the same densities of surface holes and electrons. Then, the quadratic decay channel may be representative of electron-hole recombination in the surface bands with radiative and/or nonradiative modes. The microscopic mechanism of this efficient electron-hole recombination, on the surface, is another interesting and important problem worthy of future study.

In summary, the dynamics of photogenerated electrons on Si(001)-(2×1) have been studied by means of time- and angle-resolved 2PPE at 291 K. The decay kinetics of the CBM electron population for two different excitation wavelengths, where the bulk absorption coefficients differ significantly, shows a prominent excitation-wavelength dependence. This dependence is characterized by carrier diffusion away from the surface and by efficient surface recombination. Simultaneous probing of temporal changes in electron populations at both D_{down} and the CBM has resulted in the elucidation the pathways of bulk-to-surface electron transfer. This transition occurs first to the high-lying state along the $\bar{\Gamma}-\bar{J}'$ dispersive branch of D_{down}, which is directly probed using the angle-resolved technique, followed by a fast intraband relaxation to the bottom of the surface band. Quantitative comparisons of directly monitored electron flows into D_{down} and the temporal population of the bottom of $D_{\mathrm{down}}(\bar{\Gamma})$ has revealed an efficient quadratic decay channel at the surface state.

ACKNOWLEDGMENT

This work was supported by a Specially Promoted Research of Grant-in-Aid for Scientific Research from the Ministry of Education, Science, Technology, Sports, and Culture of Japan.

[1] A. Rousse, C. Rischel, S. Fourmaux, I. Uschmann, S. Sebban, G. Grillon, Ph. Balcou, E. Förster, J. P. Geindre, P. Audebert, J. C. Gauthier, and D. Hulin, Nature (London) **410**, 65 (2001).
[2] P. B. Hillyard, K. J. Gaffney, A. M. Lindenberg, S. Engemann, R. A. Akre, J. Arthur, C. Blome, P. H. Bucksbaum, A. L. Cavalieri, A. Deb, R. W. Falcone, D. M. Fritz, P. H. Fuoss, J. Hajdu, P. Krejcik, J. Larsson, S. H. Lee, D. A. Meyer, A. J. Nelson, R. Pahl, D. A. Reis, J. Rudati, D. P. Siddons, K. Sokolowski-Tinten, D. von der Linde, and J. B. Hastings, Phys. Rev. Lett. **98**, 125501 (2007).
[3] M. Harb, R. Ernstorfer, C. T. Hebeisen, G. Sciaini, W. Peng, T. Dartigalongue, M. A. Eriksson, M. G. Lagally, S. G. Kruglik, and R. J. Dwayne Miller, Phys. Rev. Lett. **100**, 155504 (2008).
[4] E. Collet, M. H. Leme'e-Cailleau, M. Buron-Le Cointe, H. Cailleau, M. Wulff, T. Luty, S. Koshihara, M. Meyer, L. Toupet, P. Rabiller, and S. Techert, Science **300**, 612 (2003).
[5] P. Baum, Ding-Shyue Yang, and A. H. Zewail, Science **318**, 788 (2007).
[6] R. K. Raman, Y. Murooka, Chong-Yu Ruan, T. Yang, S. Berber, and D. Toma'nek, Phys. Rev. Lett. **101**, 077401 (2008).
[7] H. O. Jeschke, M. E. Garcia, and K. H. Bennemann, Phys. Rev. Lett. **87**, 015003 (2001).
[8] M. Lenner, A. Kaplan, and R. E. Palmer, Appl. Phys. Lett. **90**, 153119 (2007).
[9] F. Carbone, P. Baum, P. Rudolf, and A. H. Zewail, Phys. Rev. Lett. **100**, 035501 (2008).
[10] C. Jacoboni and L. Reggiani, Rev. Mod. Phys. **55**, 645 (1983).
[11] M. V. Fischetti, IEEE Trans. Electron Devices **38**, 634 (1991).
[12] J. R. Goldman and J. A. Prybyla, Phys. Rev. Lett. **72**, 1364 (1994).
[13] T. Sjodin, H. Petek, and H. L. Dai, Phys. Rev. Lett. **81**, 5664 (1998); Chem. Phys. **251**, 205 (2000).
[14] A. J. Sabbah and D. M. Riffe, Phys. Rev. B **66**, 165217 (2002).
[15] M. W. Rowe, H. Liu, G. P. Williams, and R. T. Williams, Phys. Rev. B **47**, 2048 (1993).
[16] N. J. Halas and J. Bokor, Phys. Rev. Lett. **62**, 1679 (1989).
[17] T. Fauster, in *Solid-State Photoemission and Related Methods: Theory and Experiment*, edited by W. Schattke and M. A. Van Hove (Wiley, New York, 2003).
[18] C. Kentsch, M. Kutschera, M. Weinelt, T. Fauster, and M. Rohlfing, Phys. Rev. B **65**, 035323 (2001).
[19] S. Ramakrishna, F. Willing, and A. Knorr, Appl. Phys. A: Mater. Sci. Process. **78**, 247 (2004).
[20] T. Ichibayashi and K. Tanimura, Phys. Rev. B **75**, 235327 (2007).
[21] T. Tabata, A. Aruga, and Y. Murata, Surf. Sci. **179**, L63 (1987).
[22] W. Mönch, *Semiconductor Surfaces and Interfaces* (Springer, New York, 1995).
[23] J. Pollmann, P. Kruger, M. Rohlfing, M. Sabisch, and D. Vogel, Appl. Surf. Sci. **104-105**, 1 (1996).
[24] M. Weinelt, M. Kutschera, T. Fauster, and M. Rohlfing, Phys. Rev. Lett. **92**, 126801 (2004).
[25] M. Weinelt, M. Kutschera, R. Schmidt, C. Orth, T. Fauster, and M. Rohlfing, Appl. Phys. A: Mater. Sci. Process. **80**, 995 (2005).
[26] S. Tanaka and K. Tanimura, Surf. Sci. **529**, L251 (2003).
[27] S. Tanaka and K. Tanimura, Surf. Sci. **593**, 26 (2005).
[28] D. E. Aspnes and A. A. Studna, Phys. Rev. B **27**, 985 (1983).
[29] M. Kutschera, M. Weinelt, M. Rohlfing, and T. Fauster, Appl. Phys. A: Mater. Sci. Process. **88**, 519 (2007).
[30] H. M. van Driel, Phys. Rev. B **35**, 8166 (1987).
[31] T. Ichibayashi and K. Tanimura, Phys. Rev. Lett. **102**, 087403 (2009).
[32] K. Tanimura and T. Ichibayashi, Proc. SPIE **7214**, 72141M (2009).